

Water Condensation in Hydrophobic Silicalite-1 Zeolite: A Molecular Simulation Study

Nicolas Desbiens, Anne Boutin, and Isabelle Demachy*

Laboratoire de Chimie Physique, Bâtiment 349, UMR 8000 CNRS and Université Paris-Sud, 91405 Orsay, France

Received: July 28, 2005; In Final Form: October 7, 2005

We report grand canonical Monte Carlo simulations of the gas and liquid phase adsorption of water in silicalite-1 zeolite. Simple but effective models and simulation methods, found useful for studying gas adsorption in nanoporous materials, have been extended to describe the intrusion/extrusion cycle of water in this hydrophobic solid. The picture of water confined to hydrophobic spaces of nanoscopic dimensions that emerges from this study is one of a strongly depleted and highly inhomogeneous fluid.

1. Introduction

Zeolites are crystalline aluminosilicate nanoporous materials that are widely used as selective catalysts and adsorbents.^{1,2} In many applications such as molecular separations, the zeolitic materials used in the industrial process exhibit a low framework Si:Al ratio (typically between 1 and 3). The resulting high extraframework cationic content makes these materials highly hydrophilic. The need exists however for designing hydrophobic adsorbents that could be used for gas separation in the presence of water (an example of this kind is the organic solvent separation from moist gas streams³). Dealuminated zeolites are not hydrophobic enough,³ due to their high amount of framework defects, and solid-state chemists have thus concentrated in the direct synthesis of all-silica zeolites (Si:Al = ∞), such as silicalite-1,^{4,5} zeolite-beta,⁶ and zeolite A (ITQ-29).⁷

Recently, a potential new field of application for these hydrophobic zeolites was suggested.^{8–10} It was shown that storage or dissipation of mechanical energy could be achieved by forced intrusion/extrusion of water into/from these nanoporous solids. At room temperature, water condensation occurred upon intrusion into silicalite-1 zeolite at a hydraulic pressure of about 100 MPa. A spontaneous capillary evaporation (drying) took place upon release of the pressure. Similar behavior was observed very recently in the case of hydrophobized MCM-41 mesoporous materials.¹¹ Interestingly, the intrusion/extrusion cycle was accompanied by a hysteresis effect in the latter case, but not in the former one. Situations were also encountered in which no extrusion of water took place upon release of the pressure (zeolite-beta and wide-pore MCM-41).^{8–11}

To shed light on these phenomena we have undertaken a Monte Carlo simulation study of gas as well as liquid water adsorption in silicalite-1 zeolite. We have been able to reproduce the experimentally observed liquid-phase intrusion/extrusion of water into/from this hydrophobic solid and thus to investigate the structural and thermodynamic properties of the condensed confined water at the molecular level. A preliminary report of this work, together with some new experimental data, has been published earlier.¹² In the present article we describe in detail the molecular simulation models and provide a full account, analysis, and discussion of the simulation results.

TABLE 1: Cell Parameters of Silicalite-1 Zeolite

	<i>a</i> (Å)	<i>b</i> (Å)	<i>c</i> (Å)	α (deg)	β (deg)	γ (deg)
<i>Pnma</i> ¹³	20.070	19.920	13.420	90.0	90.0	90.0
<i>P2₁n11</i> ¹⁴	20.107	19.879	13.369	90.67	90.0	90.0

2. Models and Methods

2.1. Silicalite-1 Model. We used a rigid zeolite framework and used the atomic coordinates of the orthorhombic (*Pnma*) structure determined by Olson et al.¹³ The unit cell parameters are given in Table 1. Another crystallographic structure is known to exist (monoclinic *P2₁n11*),¹⁴ but it has not been clearly demonstrated to date which is the most stable phase for a given thermodynamic parameters state and for a given loading of adsorbed molecular fluid. The unit cell parameters and porous volume of the two phases are close to each other (see Table 1). We decided to use an orthorhombic model, as in most of the previous molecular simulation studies of MFI-type zeolites.

An orthorhombic unit cell is composed of 96 SiO₂ units. The Atlas of Zeolite structure types¹⁵ denotes this silicalite-1 structure (MFI structure type) as being made of elliptical straight channels (SC) with a diameter of 5.1 × 5.5 Å, which runs in the direction of the *y*-axis, zigzag channels (ZC) with a diameter of 5.3 × 5.6 Å parallel to the *xz* plane, and intersections (I). There are four SC, ZC, and I per unit cell. A sketch of the interconnected pore channels in silicalite-1 is shown in Figure 1.

2.2. Force Field. The host/guest potential is of the “Kiselev type”.^{16,17} It contains a single effective Lennard-Jones term that acts between the oxygen atoms of the framework and the oxygen atoms of the guest water molecules, together with a Coulombic term that acts between the partial charges of the silicon and oxygen atoms and those of the guest molecules. We used the Lennard-Jones parameters for the zeolite oxygen atoms obtained from our previous work on the adsorption of hydrocarbons in silicalite-1¹⁸ ($\sigma_{\text{O}} = 3.00$ Å; $\epsilon_{\text{O}} = 93.53$ K), together with the Lorentz–Berthelot combining rules.

Several atomic partial charges were tested for the guest zeolite atoms, with the constraint $q_{\text{Si}} = -0.5q_{\text{O}}$, since the purely SiO₂ framework is neutral overall. There is an ongoing debate in the literature about the partial charge that a silicon atom should bear in silica-based materials.¹⁹ Atomic charges have been reported in the range of +4 to +0.5 (in units of elementary charge) depending on the computational method used, while experimental diffraction studies gave 1.17 ± 0.15^{20} and $1.2 \pm$

* To whom correspondence should be addressed. E-mail: demachy@lcp.u-psud.fr.

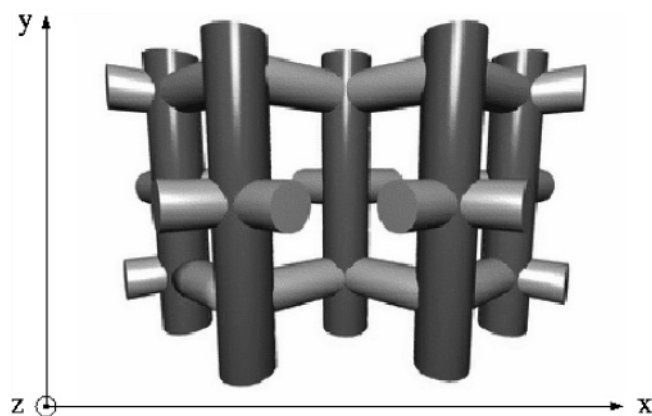


Figure 1. View of the interconnected pore channels in silicalite-1 (MFI type structure).

TABLE 2: Atomic Charges of Silicon Atom in Silicates, Aluminosilicates, or Siliceous Compounds Obtained by Theoretical Methods

q_{Si}	method	system
+0.52 ²⁶ /+ 1.1 ²⁷	SCF/Mulliken	silicic acids/silicic clusters
+1.49 ^{28,29} /+1.4 ³⁰	periodic HF/Mulliken	silicalite-1/ α -quartz
+1.4 ³²	MP ₂ /CHELPG	silicic acids
+2.4 ²⁵	SCF/empirical	H ₄ SiO ₄ , disilicalite
+3.3 ²⁴	DFT/LDA/Mulliken	ferrosilicic compounds/mica
+1.93 ³³ /+1.63 ³⁴	EEM	silicalite-1
+1.1 ¹⁹	extended Born model	SiO ₂ , mica and montmorillonite

0.1.^{21–22} The +4.0 value is the formal charge of a silicon atom. Simple electronegativity differences indicate that the Si–O bond is roughly 50% ionic, which implies a partial charge of +2.0.²³ Ab initio methods enable computation of the electron density, which can then be partitioned into atomic charges. An alternative way is to use semiempirical equilibration methods, such as the very popular electronegativity equalization method (EEM).³¹ Some literature values^{19,24–30,32–34} are reported in Table 2.

Given the large uncertainty on the partial charge values of the framework atoms, we have chosen here to compute the Coulombic part of the guest–host potential, using three different test charges for the silicon atom: 2.0, 1.4, and 1.2. The guest–host interactions were calculated on a grid of points prior to the simulations. The grid mesh is ~ 0.2 Å in the three space directions. The Ewald summation technique was used to compute the electrostatic energy. The Ewald parameters $k_{\text{max}} = 15$ and $n_{\alpha} = 3$, were used for both the electrostatic grid calculation and the simulations.

For the guest–guest potential, we have tested four different two-body semiempirical rigid water models, the so-called TIP4P,^{35a} MSPC/E,³⁶ TIP5P,^{37a} and DEC.³⁸ The first three models consist of a Lennard-Jones term that acts between oxygen atoms only, and a Coulombic term that acts between partial charges that are placed on the hydrogen atoms and either on the oxygen atom or at some point away, but close to the oxygen atom of the water molecule. The latter model is a little bit more complex since it employs Gaussian distributed charges. We have reported in Table 3 the computed saturated vapor pressure for these four models, at 300 K. The TIP4P and MSPC/E models are known to reproduce rather well the density and the local structure ($g(r)$) of liquid water. As shown in Table

3, they provide saturated vapor pressure values that are 40–50% away from the experimental value. This can be considered as a fair agreement, given the well-known difficulty in reproducing all the water properties with a single, semiempirical potential. As far as the saturated vapor pressure is concerned, the TIP5P and DEC potentials are worse than the first two potentials by a factor of ~ 5 . Recently a reparametrized version of the TIP5P model was suggested,^{37c} but the corresponding saturation vapor pressure is not known. Because of this, we shall mainly use the TIP4P and MSPC/E potentials for the liquid state adsorption simulations described further below. It is worth noticing that TIP4P was recently shown to provide a fairly good description of the adsorption of water in faujasite zeolites.^{39–41}

2.3. Simulation Method. Adsorption isotherms were computed using bias grand canonical Monte Carlo (GCMC) simulations.^{42–43} We simulated a box of eight unit cells of silicalite-1 with periodic boundary conditions. We used the preinsertion⁴⁴ and the orientational^{45,46} bias move for the molecular insertion MC step, to accelerate the convergence of the simulation runs. Each run lasted for some 30 million steps in order to equilibrate the system, followed by 15 million steps for the data acquisition.

2.4. Water Chemical Potential in the Gas and in the Liquid Phase. Our aim in this work was to compute the gas-phase as well as the liquid-phase adsorption of water in silicalite-1 at room temperature. GCMC simulations were thus performed, at each pressure, by exchanging molecules between the zeolite sample and a fictitious external gas reservoir at the same chemical potential as the gas or liquid water at the pressure of interest. For this, we need to know the $\mu(P)$ relationship for the bulk water model used in the simulations.

We found in the literature two ways of deriving the $\mu(P)$ relationship. Porcheron and Monson⁴⁷ integrated the Gibbs–Duhem equation to model mercury porosimetry experiments. Chempath et al.⁴⁸ used a Peng–Robinson equation of state to compute the chemical potential of the vapor in equilibrium with a liquid at a given temperature. We choose here another option, which consists of computing the $\mu(P)$ relationship from simulations. The direct calculation of the chemical potential, either from (μ, V, T) or from (N, P, T) simulations (using in this latter case the Widom test particle method), is subject to large uncertainties due to the fluctuations of the computed quantities. We have used here density as an intermediate, easy to compute, quantity. We first computed the bulk water density as a function of chemical potential (using GCMC simulations) and checked our results against the NIST experimental database values.⁴⁹ As already noticed previously^{50–52} the TIP4P and MSPC/E potentials reproduce quite well the experimental water densities at pressures up to 10^2 to 10^3 MPa. We then performed (N, P, T) simulations in order to obtain a numerical relationship between density and pressure and finally gathered all these data together to obtain the $\mu(P)$ relationship shown in Figure 2. Again, the TIP4P and MSPC/E results agree rather well with the NIST data.

2.5. Porous Volume Analysis. To be able to compute the density of the confined condensed water, once we know the average number of adsorbed molecules per unit cell, we have estimated the total accessible nanopore volume as well as the

TABLE 3: Saturated Vapor Pressure P° (Pa) of Different Water Models at 300 K

	experiments	TIP4P	MSPC/E	TIP5P	DEC
lit.	3537 ⁴⁹	4157 ^{35b} –5517 ^{35c}	2200 \pm 300 ³⁶	13112 \pm 270 ^{37b}	
this work		5300 \pm 600	1940 \pm 150	14300 \pm 3800	27790 \pm 2300

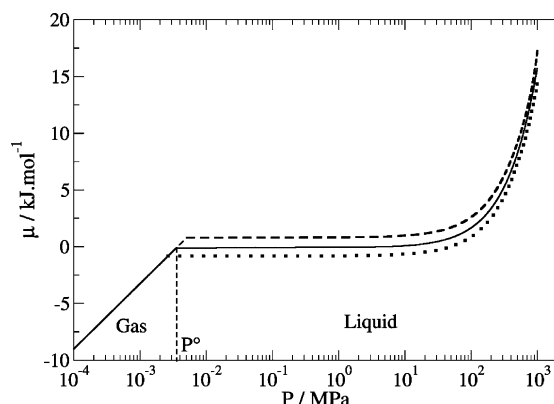


Figure 2. Chemical potential of gas and liquid water at 300 K as a function of pressure: solid line, NIST database;⁴⁹ dashed line, computed using TIP4P model (see text); dotted line, computed using MSPC/E model (see text)

subvolumes corresponding to the straight channels (SC), zigzag channels (ZC), and intersections (I) of silicalite-1.

The total accessible volume was computed using the so-called “Connolly surface”,^{53,54} which is the surface traced by the outside of a test particle “rolled” over the pore wall. The use of this method for computing nanoporous volumes has been discussed in detail by Gelb and Gubbins.⁵⁵ Using a radius of the test particle of 1.577 Å (i.e., half of the Lennard-Jones diameter of the TIP4P water model), and a radius of the framework oxygen atom of 1.5 Å, we obtained a total porous volume of 1833 Å³/unit cell (0.192 cm³·g⁻¹). This corresponds to a porosity of 34.2%. Given the somewhat arbitrary values of the parameters used for computing the Connolly volume, we estimate the uncertainty on the computed porous volume to be ±6%. The computed porosity is thus in fair agreement with the reported experimental values of 37.4⁵⁶ and 36.9%,⁸ determined from nitrogen adsorption data. In a recent theoretical study of silicalite-1, Fleys and Thompson⁵⁷ obtained a porosity of 32%, using the Connolly volume method.

We have then separately estimated the three subvolumes in the following way. A portion of a straight channel (SC) is defined as the volume between two intersections (I). These two subvolumes are physically separated by a 10 oxygen atom ring window, through which a mean surface can be easily drawn. The SC subvolume is then unambiguously defined. There is no such clear-cut separation between the zigzag channels (ZC) and the intersections. We thus had to define a physically reasonable value for the distance between the center of the intersection and an arbitrary plane that separates I from ZC (see Figure 3). We used a value of $r = 3.2 \pm 0.6$ Å to estimate the I and ZC subvolumes. The uncertainty on these latter subvolumes is on the order of 10%. We report in Table 4 the porous volumes estimated using the Connolly parameters and the method described above.

3. Results and Discussion

3.1. Gas-Phase Adsorption. As stated above in section 2.2., we have chosen to compute the Coulombic part of the guest–host potential (which is the dominant part of the guest–host interaction energy) using three different test charges for the

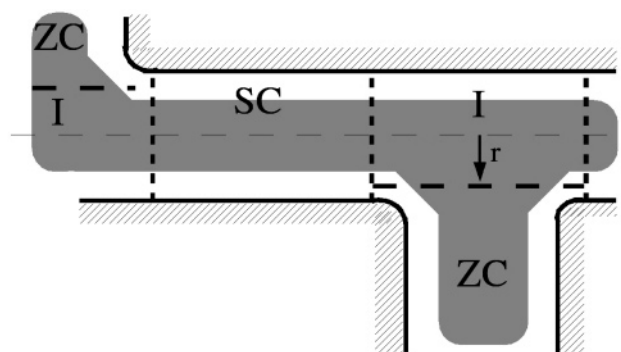


Figure 3. Schematic view of the straight channels (SC), zigzag channels (ZC), and intersection (I) subvolumes.

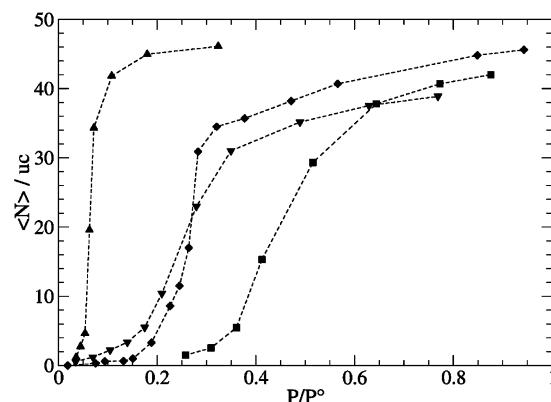


Figure 4. Gas-phase adsorption isotherms of water in silicalite-1 from GCMC simulations at 300 K for different water models and $q_{Si} = +2.0$. diamonds, TIP4P water model; squares, MSPC/E water model; triangles down, TIP5P water model; triangles up, DEC water model. Lines are guides to the eye. The P° value of each model was taken from our GCMC simulations (see Table 3).

framework silicon atom: 2.0, 1.4, and 1.2. This first part of the results section is devoted to the data obtained using $q_{Si} = 2.0$.

We report in Figure 4 the gas-phase adsorption isotherms, using the four different water force fields described above in section 2.2. In all four cases, a sigmoidal, type V isotherm is observed, with no hysteresis. The high-pressure plateau of the isotherms (40–50 molecules per unit cell) corresponds to a complete filling of the zeolite host, as we will see in the next section. The reported isotherms correspond to a condensation of water in the porous volume *below* the saturated vapor pressure. The condensation pressure ranges from 0.2 to 0.4 in reduced pressure units, depending on the potential used, except for the DEC potential for which condensation takes place at $P/P^\circ \sim 0.1$. The present findings are at variance with what was found in the experiments.

To increase the condensation pressure, and possibly observe a transition above the saturation vapor pressure, one has to modify the balance between the guest–host and guest–guest attractive interactions. We have chosen here not to modify the water model parameters and to reduce the electrostatic guest–host interaction by lowering the partial charge carried by the framework silicon atom. In the case of the TIP4P and MSPC/E water models, we found that this partial charge should be kept

TABLE 4: Computed Accessible Volumes for the Straight Channels (SC), Zigzag Channels (ZC), Intersections (I), and Total Porous Volume

	SC	ZC	I	total
porous vol (Å ³ ·uc ⁻¹)	445 ± 27	763 ± 122	625 ± 100	1833 ± 110
porous vol (cm ³ ·g ⁻¹)	0.0465 ± 0.0028	0.0797 ± 0.0127	0.0653 ± 0.0104	0.192 ± 0.012

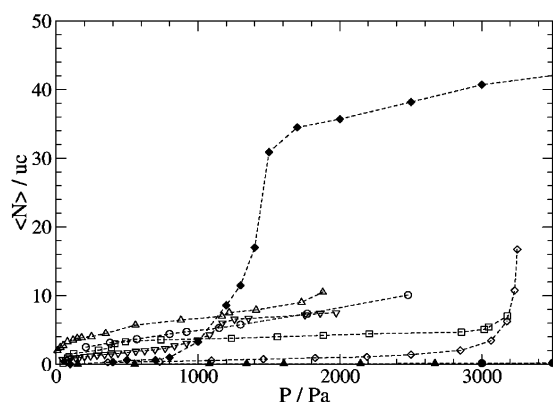


Figure 5. Gas-phase adsorption isotherms of water in silicalite-1 at 300 K: open dots, experiments;⁵⁶ open squares, experiments;¹⁰ open diamonds, experiments;⁵⁸ open triangles, experiments;⁵⁹ open triangles down, experiments;⁶⁰ full triangles, GCMC simulations;⁵⁷ full diamonds, this work (TIP4P and $q_{\text{Si}} = +2.0$); full dots, this work (TIP4P and $q_{\text{Si}} = +1.4$).

below approximately 1.7 in order to prevent a condensation phenomenon at a gas pressure below the saturation pressure of the bulk water. The liquid-phase adsorption process that occurs above the saturation vapor pressure will be described below in section 3.2.

In Figure 5, we report the computed gas-phase adsorption isotherms using the TIP4P model with $q_{\text{Si}} = 2.0$ and $q_{\text{Si}} = 1.4$, together with the gas-phase experiments found in the literature.^{10,56,58–60} The various experimental data strongly disagree with each other. At half the value of the saturated vapor pressure (~ 1700 Pa), the amount of water adsorbed in the experiments varies from one to eight molecules per unit cell. This has been tentatively attributed to a varying amount of defects in the zeolite samples.^{10,57} It is not yet clear however, what kind of defects (surface or framework defects and of which chemical nature) may lead to a weak, presumably localized, water adsorption. In this respect, it is interesting to point out that the same silicalite-1 sample, synthesized by Patarin and co-workers, displays a weak vapor phase adsorption (approximately three to four molecules/u.c.), followed by a stepwise liquid-phase condensation at high pressure¹⁰ (see next section).

To end up with the discussion of the experimental vapor phase adsorption, we suggest that the steep water uptake reported in two of the experimental studies slightly above 3000 Pa could be attributed to a capillary condensation occurring in the meso- or macroporosity of the zeolite sample.

In the model (defect-free) zeolite sample, the computed adsorption quantities, using $q_{\text{Si}} = 1.4$, are extremely low (some 0.2 molecule per unit cell). This was also the case for the GCMC results of Fleys and Thompson,⁵⁷ who used the compass force field to simulate gas-phase water adsorption in silicalite-1 (see Figure 5).

3.2. Liquid-Phase Adsorption. The simulated liquid-phase adsorption data at 300 K, using the TIP4P force field and $q_{\text{Si}} = 1.4$, are reported in Figure 6. A stepwise condensation is observed at a pressure of about 50 MPa. The agreement with the experimental intrusion pressure is quite good, given that there is only a 3% difference in the chemical potential of liquid water between 50 and 100 MPa. Very similar results were obtained using the MSPC/E water force field (see Figure 6).

An even better agreement with experimental data can be obtained by fixing an atomic charge of 1.2 on the silicon atom. The shape and the water loading of the computed intrusion isotherms are in good agreement with the recently reported

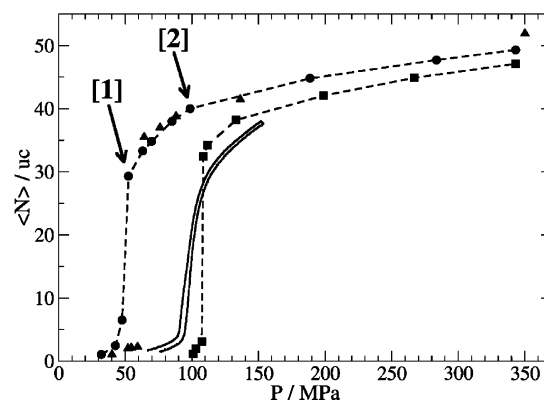


Figure 6. Liquid-phase adsorption isotherms of water in silicalite-1 at 300 K: dots, TIP4P water model for $q_{\text{Si}} = +1.4$; triangles, MSPC/E water model for $q_{\text{Si}} = +1.4$; squares, TIP4P water model for $q_{\text{Si}} = +1.2$; solid lines, intrusion/extrusion experiments.¹² Dotted lines are guides to the eyes.

experimental data.¹² This observation is remarkable given the crudeness of the model used in the simulations.

The observed first-order-like transition is reminiscent of the two-state description of the water behavior in model carbon nanotubes⁶¹ and nanoporous cylindrical channels⁶² observed recently in molecular dynamics studies. The computed isotherms shown in Figure 6 are reversible, within statistical uncertainties. This is generally what we expect for a Monte Carlo simulation, although it is known that GCMC adsorption isotherms may, in some special cases, exhibit hysteresis.⁶³ The computed isotherms displayed in Figure 6 can thus be considered as the equilibrium intrusion/extrusion curve of the model water/silicalite-1 system. It is the first time, to our knowledge, that this condensation/drying phenomenon has been reproduced theoretically.

3.3. Analysis of the Condensation Process. In this section, we examine in some detail the condensation process observed in the liquid-phase adsorption simulations. We concentrate here on the $q_{\text{Si}} = 1.4$ and water TIP4P model, since the results obtained with $q_{\text{Si}} = 1.2$ and/or the MSPC/E water models are qualitatively similar.

From the computed average number of adsorbed water molecules $\langle N \rangle$ and the estimated accessible porous volume and subvolumes, we have computed the average and subvolume densities of confined water as a function of pressure. It must be stressed here that the reported densities are strictly defined as the average number of computed adsorbed molecule in a given accessible volume, divided by this very volume. No hypothesis is made on the effective volume occupied by water molecules in the nanopores. We have checked that the accessible volume reported in section 2.5 is not only sterically but also energetically accessible for a single water molecule. This means that the overall guest–host interaction potential is attractive everywhere in the accessible volume. The density results are reported in Figure 7.

The stepwise condensation phenomenon is observed in all three regions (subvolumes) of the zeolite at a pressure of approximately 50 MPa. At this pressure (marked “1” in Figures 6 and 7) the average density of the condensed water is less than half that of the bulk water density under the same thermodynamic conditions. The condensed fluid is extremely inhomogeneous. The density in the intersections is nearly three times as large as that of the fluid in the straight or zigzag channels. The average occupancy is three water molecules at an intersection, while there is only one molecule on average in the SC or ZC. At this stage, the filling of the channels (SC or ZC) is also highly inhomogeneous. In Figure 8, we present the distributions

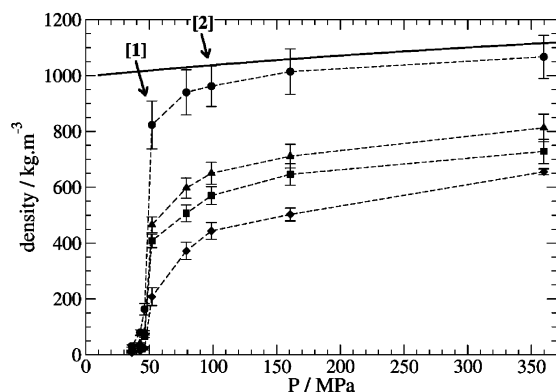


Figure 7. Density of condensed water in silicalite-1 as a function of pressure from GCMC simulations (TIP4P model and $q_{Si} = +1.4$): dots, local density in the intersections (I); squares, local density in the straight channels (SC); diamonds, local density in the zigzag channels (ZC); triangles, average confined water density; full line, bulk water density. The dotted lines are guides to the eye.

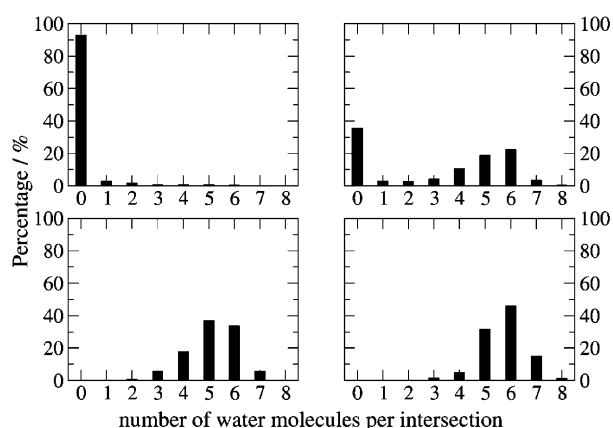


Figure 8. Distribution of adsorbed water molecules in the intersection subvolumes: top left histogram, $P = 36.3$ MPa; top right, $P = 50.2$ MPa (state “1”); bottom left, $P = 100.1$ MPa (state “2”); bottom right, $P = 360.0$ MPa.

of water molecules in the intersections at different pressure. Below the condensation pressure (top left histogram), most of the intersections are empty. At state “1” (top right histogram) 40% of the intersections are empty while the others are filled with an average of five to six molecules. There is clearly a clustering effect in this first condensation step. The formation of water clusters in silicalite-1 was already suggested in some previous molecular dynamics studies.^{64–66} The same behavior seems to hold true in the case of carbon nanopores.^{67,68} The current results are in keeping with the observation of Vaitheeswaran et al.⁶⁸ that linear chains of water molecules inside a narrow cylindrical pore are less stable than the water clusters in a spherical nonpolar cavity of comparable volume.

A second condensation regime takes place as the pressure is increased from 50 to about 100 MPa. At the point marked “2” in Figures 6 and 7, each intersection is now occupied by an average of five to six molecules (Figure 8, bottom left histogram) and the SC and ZC by two water molecules. The channel filling now becomes homogeneous, with each channel section containing approximately the same number of molecules. At this stage, the water density in the intersection has almost reached the bulk fluid value, while the density in the channels is lower by a factor close to 2 (Figure 7). This fact can be interpreted by considering that the three-dimensional-like geometry of the pore intersections enables water molecules to pile up in more or less the same way as in the bulk liquid. On the other hand, the pseudo-one-

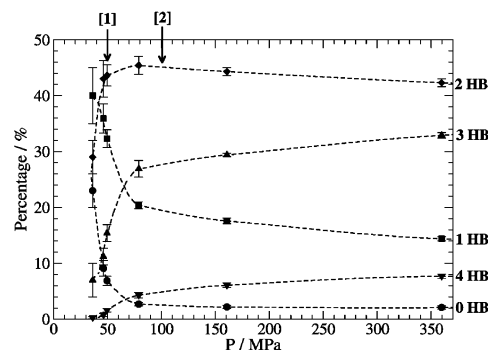


Figure 9. Percentage of molecules involved in intermolecular hydrogen bonds (HB) as a function of pressure for TIP4P water model.

dimensional channel geometry prevents such a bulklike state from being reached. It is worth mentioning that the strong depletion of fluid observed in the present simulations cannot simply be accounted for by a failure of the water force field, since the TIP4P intermolecular potential was checked to provide very accurate values for the density of bulk water at high pressure.

We have computed the average number of water molecules involved in zero, one, two, three, or four hydrogen bonds, as a function of pressure. For a hydrogen bond to exist, we use the geometrical criteria suggested by Marti⁶⁹ ($r_{O-O} < 3.6$ Å; $r_{O-H} < 2.4$ Å; $O-O/O-H$ angle $< 30^\circ$).

The results of the hydrogen bond formation are shown in Figure 9. Among the interesting features, we note that immediately below the condensation pressure, the few adsorbed molecules (i.e., less than one molecule per unit cell!) are preferably associated with each other, since only 20% of them display zero hydrogen bonds. This confirms that water condensation takes place through a cooperative clustering phenomenon. We also note the spectacular change in hydrogen bonding network between states “1” and “2”. This corresponds to the collapse of dimers and trimers into larger clusters. The average number of hydrogen bonds in the confined water reaches the value of ~ 2.3 at complete filling. This is to be compared to the value of 3–3.5 hydrogen bonds in the bulk water liquid at room temperature.

Finally, the observation of a first-order-like transition occurring *everywhere* in the porous solid, and at the same pressure is somewhat unexpected. The SC and ZC of silicalite-1 form pseudo-one-dimensional confined systems in which a first-order transition is theoretically forbidden. We presume that this could be explained by some correlation between adjacent pores, a feature that was previously suggested by Radhakrishnan and Gubbins.⁷⁰

4. Conclusion

Simple but effective models and simulation methods, found useful for studying gas adsorption in nanoporous materials, have been extended to describe the intrusion/extrusion cycle of a nonwetting fluid in a hydrophobic solid. We have reproduced for the first time the condensation transition of water in silicalite-1 zeolite at room temperature. The picture of water confined to hydrophobic spaces of nanoscopic dimensions that emerges from this study is one of a strongly depleted and highly inhomogeneous fluid.

Acknowledgment. Michel Soulard and Joël Patarin are gratefully acknowledged for advise and numerous fruitful discussions regarding the hydrophobic zeolitic materials and

their experimental intrusion–extrusion data. Florence Porcher and Claude Lecomte are gratefully acknowledged for providing us with experimental atomic partial charges prior to publication. Bertrand Guillot is gratefully acknowledged for numerous discussions on the water potentials. Randy Snurr is acknowledged for fruitful discussions and correspondence. Special thanks are due to Alain Fuchs for his support.

References and Notes

- (1) Auerbach, S. M.; Carrado, K. A.; Dutta, P. K., Eds. *Handbook of Zeolite Science and Technology*; Marcel Dekker: New York, 2003.
- (2) Crystalline and organized porous solids (thematic issue). Patarin, J.; Gies, H., Eds. *C. R. Chim.* **2005**, *8* (3–4).
- (3) Stelzer, J.; Paulus, M.; Hunger, M.; Weitkamp, J. *Microporous Mesoporous Mater.* **1998**, *22*, 1–8.
- (4) Flanigen, E. M.; Bennett, J. M.; Grose, R. W.; Cohen, J. P.; Patton, R. L.; Kirchner, R. M.; Smith, J. V. *Nature* **1978**, *271*, 512–516.
- (5) Guth, J.-L.; Kessler, H.; Wey, R. In Proceedings of the 7th International Zeolite Conference, Tokyo, Japan, **1986**; *Studies in Surface Science and Catalysis*; Murakami, Y., Iijima, A., Ward, J. W., Eds.; Elsevier: Amsterdam, 1986; pp 121–128.
- (6) Cambor, M. A.; Corma, A.; Valencia, S. *Chem. Commun.* **1996**, 2365–2366.
- (7) Corma, A.; Rey, F.; Rius, J.; Sabater, M. J.; Valencia, S. *Nature* **2004**, *431*, 287–290.
- (8) Eroshenko, V.; Regis, R.-C.; Soulard, M.; Patarin, J. *J. Am. Chem. Soc.* **2001**, *123*, 8129–8130.
- (9) Eroshenko, V.; Regis, R.-C.; Soulard, M.; Patarin, J. *C. R. Phys.* **2004**, *3*, 111–119.
- (10) Soulard, M.; Patarin, J.; Eroshenko, V.; Regis, R.-C. In Proceedings of the 14th International Zeolite Conference, Cape Town; Van Steen, E., et al., Eds.; **2004**, 1830–1837.
- (11) Lefevre, B.; Saugey, A.; Barrat, J.-L.; Bocquet, L.; Charlaix, E.; Gobin, P. F.; Vigier, G. *J. Chem. Phys.* **2004**, *120*, 4927–4938.
- (12) Desbiens, N.; Demachy, I.; Fuchs, A. H.; Kirsch-Rodeschini, H.; Soulard, M.; Patarin, J. *Angew. Chem., Int. Ed.* **2005**, *44*, 5310–5313.
- (13) Olson, D. H.; Kokotailo, G. T.; Lawton, S. L.; Meier, W. M. *J. Phys. Chem.* **1981**, *85*, 2238–2243.
- (14) van Koningsveld, H.; Hansen, J. C.; van Bekkum, H. *Zeolites* **1990**, *10*, 235–242.
- (15) Baerlocher, Ch.; Meier, W. M.; Olson, D. H. *Atlas of Zeolite Framework Types*, 5th rev. ed.; Elsevier: Amsterdam, 2001. <http://www.iza-structure.org>.
- (16) Bezus, A.; Kiselev, A. V.; Lopatkin, A. A.; Du, P. Q. *J. Chem. Soc., Faraday Trans.* **1978**, *74*, 367–379.
- (17) Fuchs, A. H.; Cheetham, A. K. *J. Phys. Chem. B* **2001**, *105*, 7375–7383.
- (18) Pascual, P.; Ungerer, P.; Tavitian, B.; Pernot, P.; Boutin, A. *Phys. Chem. Chem. Phys.* **2003**, *5*, 3684–3693.
- (19) Heinz, H.; Suter, U. W. *J. Phys. Chem. B* **2004**, *108*, 18341–18352.
- (20) Belokoneva, E. L.; Gubina, Y. K.; Forsyth, J. B.; Brown, P. J. *J. Phys. Chem. Min.* **2002**, *29*, 430–438.
- (21) Thong, N.; Schwarzenbach, D. *Acta Crystallogr., Sect. A* **1979**, *A35*, 658–664.
- (22) Porcher, F. Doctorate Thesis, University of Nancy, France 1998.
- (23) Porcher, F.; Souhassou, M.; Dusauroy, Y.; Lecomte, C. Unpublished results.
- (24) Gibbs, G. V.; Downs, J. W.; Boisen, M. B., Jr. *Rev. Mineral.* **1994**, *29*, 331–368.
- (25) Terra, J.; Ellis, D. E. *Phys. Rev. B* **1997**, *56*, 1834–1847.
- (26) van Beest, B. W.; Kramer, G. J.; van Santen R. A. *Phys. Rev. Lett.* **1990**, *64*, 1955–1958.
- (27) Hill, J.-R.; Sauer, J. *J. Phys. Chem.* **1994**, *98*, 1238–1244.
- (28) Grigoras, S.; Lane, T. H. *J. Comput. Chem.* **1988**, *9*, 25–39.
- (29) White, J. C.; Hess, A. C. *J. Phys. Chem.* **1993**, *97*, 8703–8706.
- (30) Larin, A. V.; Vercauteren, D. P. *Int. J. Inorg. Mater.* **1999**, *1*, 201–207.
- (31) (a) Dovesi, R.; Pisani, C.; Roetti, C.; Silvi, B. *J. Chem. Phys.* **1987**, *86*, 6967–6971.
- (32) (a) Mortier, W. J.; Ghosh, S. K.; Shankar, S. *J. Am. Chem. Soc.* **1986**, *108*, 4315–4320. (b) Rappé, A. K.; Goddard, W. A., III *J. Phys. Chem.* **1991**, *95*, 3358–3363.
- (33) (a) Jorgensen, W. L.; Chandrasekhar, J.; Madura, J. D.; Impey, R. W.; Klein, M. L. *J. Chem. Phys.* **1983**, *79*, 926–935. (b) Lisal, M.; Smith, W. R.; Nezbeda, I. *Fluid Phase Equilib.* **2001**, *181*, 127–146; (c) Vorholtz, J.; Harismiadis, V. L.; Rumpf, B.; Panagiotopoulos, A. Z.; Maurer, G. *Fluid Phase Equilib.* **2000**, *170*, 203–234.
- (34) Uytterhoeven, L.; Mortier, W. J.; Geerlings, P. *J. Phys. Chem. Solids* **1989**, *50*, 479–486.
- (35) (a) Jorgensen, W. L.; Jorgensen, W. L. *J. Chem. Phys.* **2000**, *112*, 8910–8922. (b) Lisal, M.; Kolofa, J.; Nezbeda, I. *J. Chem. Phys.* **2002**, *117*, 8892–8897. (c) Rick, S. W. *J. Chem. Phys.* **2004**, *120*, 6085–6093.
- (36) Boulougouris, G. C.; Economou, I. G.; Theodorou, D. N. *J. Phys. Chem. B* **1998**, *102*, 1029–1035.
- (37) (a) Mahoney, M. W.; Jorgensen, W. L. *J. Chem. Phys.* **2000**, *112*, 8910–8922. (b) Lisal, M.; Kolofa, J.; Nezbeda, I. *J. Chem. Phys.* **2002**, *117*, 8892–8897. (c) Rick, S. W. *J. Chem. Phys.* **2004**, *120*, 6085–6093.
- (38) Guillot, B.; Guissani, Y. *J. Chem. Phys.* **2001**, *114*, 6720–6733.
- (39) Beauvais, C.; Boutin, A.; Fuchs, A. H. *Chem. Phys. Chem* **2004**, *5*, 1791–1793.
- (40) Beauvais, C.; Boutin, A.; Fuchs, A. H. *Adsorption* **2005**, *11*, 279–282.
- (41) Beauvais, C.; Boutin, A.; Fuchs, A. H. *C. R. Chimie* **2005**, *8*, 485–490.
- (42) Nicholson, D.; Parsonage, N. G. *Computer Simulation and the Statistical Mechanics of Adsorption*; Academic Press: New York, 1982.
- (43) Frenkel, D.; Smit, B. *Understanding Molecular Simulations. From Algorithms to Applications*, 2nd ed.; Academic Press: London, 2002.
- (44) Mackie, A. D.; Tavitian, B.; Boutin, A.; Fuchs, A. H. *Mol. Simul.* **1997**, *19*, 1–15.
- (45) Cracknell, R. F.; Nicholson, D.; Parsonage, N. G.; Evans, H. *Mol. Phys.* **1990**, *71*, 931–943.
- (46) Lachet, V.; Boutin, A.; Tavitian, B.; Fuchs, A. H. *J. Phys. Chem. B* **1998**, *102*, 9224–9233.
- (47) Porcheron, F.; Monson, P. *Langmuir* **2004**, *20*, 6482–6489.
- (48) Chempath, S.; Denayer, J. F. M.; De Meyer, K. M. A.; Baron, G. V.; Snurr, R. Q. *Langmuir* **2004**, *20*, 150–156.
- (49) NIST Chemistry Webbook (<http://webbook.nist.gov/chemistry>).
- (50) Zhang, Z. G.; Duan, Z. H. *Phys. Earth Planet. Inter.* **2005**, *149*, 335–354.
- (51) Brodholt, J.; Wood, B. J. *J. Geophys. Res.* **1993**, *98*, 519–536.
- (52) Kalinichev, K. A.; Gorbaty, Y. E.; Okhulkov, A. V. *J. Mol. Liq.* **1999**, *82*, 57–72.
- (53) Connolly, M. L. *J. Appl. Crystallogr.* **1983**, *16*, 548–558.
- (54) Connolly, M. L. *J. Am. Chem. Soc.* **1985**, *107*, 1118–1124.
- (55) Gelb, L. D.; Gubbins, K. E. *Langmuir* **1998**, *14*, 2097–2111.
- (56) Giaya, A.; Thompson, R. W., *Microporous Mesoporous Mater.* **2002**, *55*, 265–274.
- (57) Fleys, M.; Thompson, R. W. *J. Chem. Theory Comput.* **2005**, *1*, 453–458.
- (58) Oumi, Y.; Miyajima, A.; Miyamoto, J.; Sano, T. *Stud. Surf. Sci. Catal.* **2002**, *142*, 1595–1602.
- (59) Kuznetsov, B. V.; Rakhmanova, T. A. *Russ. J. Phys. Chem.* **2001**, *75*, 933–938.
- (60) Olson, D. H.; Haag, W. O.; Borghard, W. S. *Microporous Mesoporous Mater.* **2000**, *35–36*, 435–446.
- (61) Hummer, G.; Rasaiah, J. C.; Noworyta, J. P. *Nature* **2001**, *414*, 188–190.
- (62) Allen, R.; Hansen, J. P.; Melchionna, S. *J. Chem. Phys.* **2003**, *119*, 3905–3919.
- (63) Woo, H.-J.; Monson, P. *Phys. Rev. E* **2003**, *67*, 041207.
- (64) Demontis, P.; Stara, G.; Suffritti, G. B. *J. Phys. Chem. B* **2003**, *107*, 4426–4436.
- (65) Bussai, C.; Fritzsche, S.; Haberlandt, R.; Hannongbua, S. *J. Phys. Chem. B* **2003**, *107*, 12444–12450.
- (66) Smirnov, K. S.; Bougeard, D. *Chem. Phys.* **2003**, *292*, 53–70.
- (67) Ohba, T.; Kanoh, H.; Kaneko, K. *J. Am. Chem. Soc.* **2004**, *126*, 1560–1562; *Nano Lett.* **2005**, *5*, 227–230.
- (68) Vaitheeswaran, S.; Yin, H.; Rasaiah, J. C.; Hummer, G. *Proc. Natl. Acad. Sci. U.S.A.* **2004**, *101*, 17002–17005.
- (69) Marti, J.; Padro, J. A.; Guardia, E. *J. Chem. Phys.* **1996**, *105*, 639–649.
- (70) Radhakrishnan, R.; Gubbins, K. E. *Phys. Rev. Lett.* **1997**, *79*, 2847–2850.